

Token Entropy Regularization for Multi-modal Antenna Affiliation Identification

Dong Chen^{1,2}, Ruoyu Li¹, Xinyan Zhang¹, Jialei Xu¹, Ruoseng Zhao^{1,3}, Zhikang Zhang¹, Lingyun Li¹, Zizhuang Wei¹

¹Huawei

²The University of Hong Kong

³The Chinese University of Hong Kong, Shenzhen
olichen@connect.hku.hk, weizizhuang@huawei.com

Abstract

Accurate antenna affiliation identification is crucial for optimizing and maintaining communication networks. Current practice, however, relies on the cumbersome and error-prone process of manual tower inspections. We propose a novel paradigm shift that fuses video footage of base stations, antenna geometric features, and Physical Cell Identity (PCI) signals, transforming antenna affiliation identification into multi-modal classification and matching tasks. Publicly available pretrained transformers struggle with this unique task due to a lack of analogous data in the communications domain, which hampers cross-modal alignment. To address this, we introduce a dedicated training framework that aligns antenna images with corresponding PCI signals. To tackle the representation alignment challenge, we propose a novel Token Entropy Regularization module in the pretraining stage. Our experiments demonstrate that TER accelerates convergence and yields significant performance gains. Further analysis reveals that the entropy of the first token is modality-dependent. Code will be made available upon publication.

1 Introduction

Accurate calibration of antenna parameters is essential for network optimization but currently relies on inefficient manual tower surveys [Aliu *et al.*, 2012; Shoaib *et al.*, 2024]. These surveys are challenging due to the large number of visually similar antennas installed at height. The Physical Cell Identity (PCI) signal offers a promising solution to this problem [Narmanlioglu and Zeydan, 2018]. As a unique identifier in 4G and 5G networks, the PCI signals allow user devices to synchronize with a cell, thereby providing a direct digital fingerprint that links radio signals to their source antenna [Qi *et al.*, 2017; Abozariba *et al.*, 2025]. Despite this potential, current automation efforts remain inadequate [Wang *et al.*, 2015]. Existing visual analysis methods fail to solve the underlying parameter-matching problem, while multi-modal AI lacks a dedicated paradigm to leverage communication signals like the PCI for this specific calibration task [Plested and Gedeon, 2022; Singh *et al.*, 2022].

End-to-end models often struggle to align multi-modal features, and existing pretrained large models lack specialization for communication network tasks [Huang *et al.*, 2024; Cheng *et al.*, 2024]. To address this gap, we propose a multi-modal fusion matching scheme to associate devices with their signals. Our training paradigm consists of two sequential phases. First, we employ CLIP-based contrastive learning to establish an initial alignment between visual antenna features and their corresponding PCI-level signals [Chen *et al.*, 2024; Liu *et al.*, 2025; Wang *et al.*, 2025]. Subsequently, a fine-tuning phase adapts these pretrained representations to the practical challenge of matching PCI signals to an unknown and variable set of antenna devices.

To also address representation learning with limited data, we draw inspiration from sparse rate reduction, which maximizes information gain through a coding rate function to facilitate representation learning [Yu *et al.*, 2023; Hu *et al.*, 2024]. This principle has been explored in the Coding Rate Reduction Transformer (CRATE), a transformer-like model that learns compressed and sparse representations [Yu *et al.*, 2023]. Building on this foundation, we introduce a Token Entropy Regularization (TER) module. TER consists of Enhanced Token Entropy (ETE) layer, which computes the entropy of token representations along the channel axis to assess encoding complexity, and a Token Entropy Loss (TEL) function, which acts as an external regularizer.

In summary, this paper has the following contributions:

(1) A Novel Problem Formulation and Foundational Paradigm: We are the first to formally define antenna affiliation identification as an open-world multi-modal matching task, bridging antenna classification and matching tasks. Departing from prior vision-only or generic multimodal methods, we introduce the first paradigm that integrates visual antenna data with domain-specific Physical Cell Identity (PCI) signals, establishing a new direction for data-driven network optimization.

(2) Introducing an Innovative Module for Feature Alignment: To address the core challenge of aligning heterogeneous data, we propose a Token Entropy Regularization (TER) module. This framework provides a novel, theoretically-grounded method for disciplined and effective fusion of visual and signal representations, advancing multi-modal learning methodology.

(3) A Validated, Efficient Pathway for Practical Deploy-

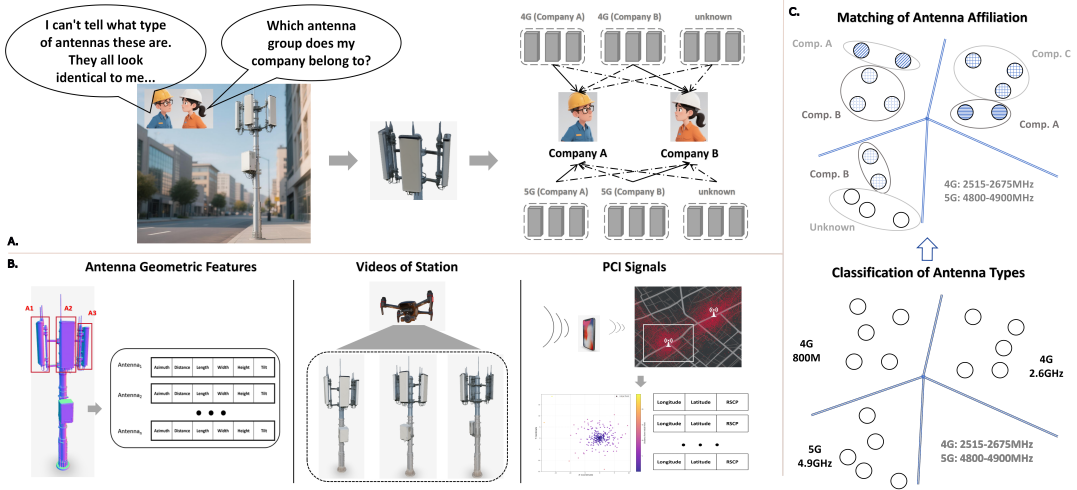


Figure 1: Schematic diagram of the multi-modal antenna affiliation identification framework. (A) The practical needs of identifying antenna affiliations. (B) A multi-modal approach is proposed with base station videos, antenna geometric features, and PCI signals. (C) The task is achieved through a two-stage training process: classifying antenna types, and matching affiliations.

ment: We demonstrate an efficient training strategy combining multimodal pretraining with targeted fine-tuning. This approach enables robust, data-efficient antenna-signal matching with substantial performance gains for 4G/5G networks, underscoring its direct viability for real-world deployment.

2 Related Work

2.1 Multi-modal Encoders

The dominance of Convolutional Neural Networks (CNNs) for visual recognition was challenged by the Vision Transformer (ViT) [Dosovitskiy *et al.*, 2020], which established the foundation by applying a pure transformer architecture directly to image patches. Subsequent work focused on improving ViT’s efficiency and adaptability for vision-specific tasks. The Data-efficient Image Transformer (DeiT) [Touvron *et al.*, 2021] introduced distillation strategies to train ViTs effectively on ImageNet alone. More importantly, hierarchical architectures like the Swin Transformer [Liu *et al.*, 2021] and the Pyramid Vision Transformer (PVT) [Wang *et al.*, 2021; Wang *et al.*, 2022] reintroduced inductive biases for multi-scale processing, enabling their use as general-purpose backbones for dense prediction. This period also saw fruitful co-evolution with modernized CNNs like ConvNeXt [Liu *et al.*, 2022b] and alternative architectures like MLP-Mixer [Tolstikhin *et al.*, 2021].

The transformer paradigm was successfully extended to video by modelling spatiotemporal relationships. Models like TimeSformer [Bertasius *et al.*, 2021], ViViT [Arnab *et al.*, 2021], and Video Swin Transformer [Liu *et al.*, 2022a] introduced novel attention mechanisms across frames, while hierarchical models like MViT [Fan *et al.*, 2021] offered integrated multiscale video understanding.

Beyond pixels, this unified architecture proved remarkably versatile. For other modalities, such as 3D point clouds, specialized encoders like the Point Transformer [Zhao *et al.*,

2021] were developed, while the vanilla Transformer encoder [Vaswani *et al.*, 2017] itself served as a powerful, permutation-invariant backbone for diverse structured data, from sensor signals (e.g., PCI points) to geometric features.

Two major learning paradigms on these backbones have driven progress. In self-supervised learning, masked autoencoding methods like MAE [He *et al.*, 2022] and knowledge distillation approaches like DINoV3 [Oquab *et al.*, 2023] have learned rich, general-purpose visual features from pixels alone. In multimodal learning, contrastive models like CLIP [Radford *et al.*, 2021] and its more efficient successor SigLIP [Zhai *et al.*, 2023] aligned visual and textual spaces, enabling zero-shot transfer. This trend towards joint representation learning has culminated in models like ImageBind [Girdhar *et al.*, 2023], which embeds multiple modalities (image, text, audio, depth, etc.) into a single, shared space, pushing the unified transformer paradigm to its logical extreme.

2.2 Token Entropy Utilization

Token entropy, which quantifies the information complexity or uncertainty of a token, has become a pivotal tool for analyzing and optimizing transformer-based models. It is widely studied for applications such as token selection [Marin *et al.*, 2021; Wu *et al.*, 2023], compression and pruning [Omri *et al.*, 2025; Song and others, 2024], to improve efficiency without sacrificing performance.

Beyond efficiency, token entropy provides critical insights for model refinement. In reasoning tasks, research shows that a minority of high-entropy “forking tokens” drive most performance gains, enabling selective optimization that matches full-parameter training efficiency [Wang and others, 2025]. For long-context modeling, frameworks like Sir-LLM leverage token entropy to identify and retain high-information phrases, significantly improving long-term memory in streaming dialogues without fine-tuning [Yao *et al.*, 2024].

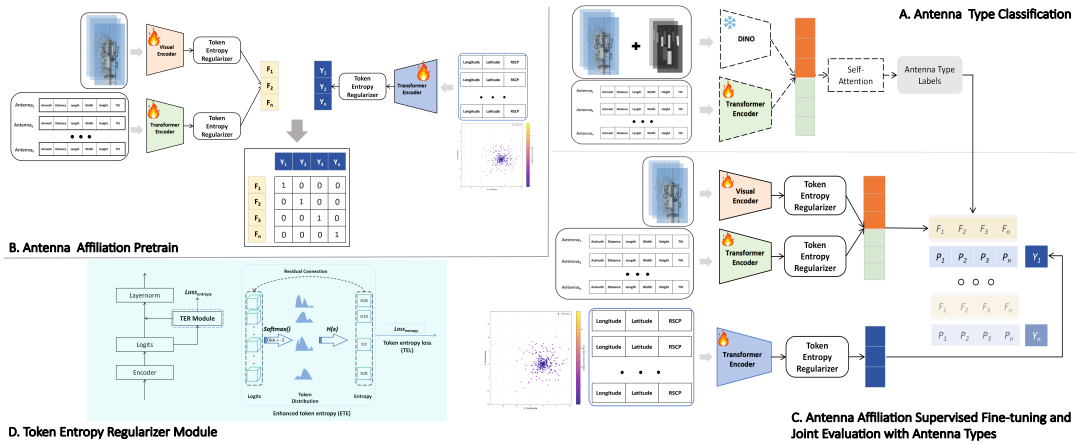


Figure 2: An overview of the proposed multimodal framework for antenna affiliation identification. (A) Antenna type classification via a supervised DINOv3-Transformer. (B, C) The antenna affiliation task comprising a pretraining stage followed by supervised fine-tuning under different data-matching conditions. (D) The Token Entropy Regularization (TER) module, which encourages model convergence by regularizing the distribution of token representations.

The most advanced applications involve structured token aggregation rather than simple selection. Researches indicate that simple cluster-level token merging, which groups semantically similar tokens, often surpasses more complex selection methods that suffer from information loss or implementation overhead [Omri *et al.*, 2025; Zeng *et al.*, 2025]. This principle aligns with findings from token merging literature, where bipartite matching approaches like ToMe demonstrate that preserving token diversity through merging is more effective than outright discarding tokens [Bolya and Hoffman, 2023].

2.3 Sparse Rate Reduction

Sparse rate reduction offers a principled methodology for learning sparse, discriminative, and diverse representations by maximizing the coding rate reduction [Yu *et al.*, 2017; Hu *et al.*, 2024]. Building on this perspective, white-box architectures such as CRATE formalize the process as iterative compression where data are progressively mapped into a sparse and structured feature space [Yu *et al.*, 2023]. In parallel, recent work on token entropy regularization adopts a complementary and optimization-based view, directly shaping the output distribution by penalizing high Shannon entropy at the token level so that the model concentrates probability mass on a few confident or semantically salient tokens [Correia *et al.*, 2019].

By analogy to learned compressed sensing, this can be viewed as training the network to allocate its representational bandwidth to the most informative coordinates: token entropy regularization encourages the model to select and amplify a small subset of content-bearing tokens that are sufficient for accurate semantic reconstruction, while suppressing redundant or background tokens that contribute little to the downstream objective [Gao *et al.*, 2025; Correia *et al.*, 2019]. The result is an adaptive, content-aware sparsity pattern in which the effective support of the representation varies with the input, much like adaptive measurement schemes in compressive imaging that focus sensing resources on salient regions,

thereby improving both interpretability and efficiency without sacrificing predictive performance [Zhu *et al.*, 2015].

3 Methodology

Following the task formulation in section 3.1, section 3.2 details the multi-modal data acquisition process. Subsequently, Section 3.3 introduces the proposed Token Entropy Regularizer, whose role in the framework in Figure 2d. Finally, the overall pipeline for the antenna affiliation task is presented, which comprises antenna type classification (Figure 2a) and is trained using a two-stage strategy (Figure 2b, c). A comparison with end-to-end training is also provided, with detailed implementations available in the supplementary materials.

3.1 Task Formulation

The core problem addressed in this work is establishing reliable correspondence between physical antenna devices observed in the wild and their unique communication signatures, particularly the Physical Cell Identity (PCI). Traditional approaches rely on manual tower-climbing surveys, which are labour-intensive, error-prone, and impractical for large-scale networks. We redefine this practical engineering challenge as an open-world multi-modal matching problem in computer vision and signal processing.

Formally, our antenna affiliation identification task can be formulated as follows: given a set of visual observations $\mathcal{V} = \{v_1, v_2, \dots, v_M\}$ containing M antenna devices from station videos or images, and a set of PCI signals $\mathcal{S} = \{s_1, s_2, \dots, s_N\}$ detected from the same station, the objective is to learn a matching function $f : \mathcal{V} \times \mathcal{S} \rightarrow [0, 1]$ that determines whether antenna device v_i corresponds to PCI signal s_j . This formulation transforms the practical antenna affiliation identification problem into a multi-modal classification and matching paradigm.

The inputs to our system comprise three complementary modalities:

- **Visual data** \mathcal{V} : Raw video footage or images capturing antenna installations at base station sites, from which individual antenna devices are extracted.
- **Geometric features** \mathcal{G} : Structured representations of antenna physical attributes, including dimensions, shape characteristics, and installation parameters.
- **PCI signals** \mathcal{S} : Digital identifiers by cellular antennas that serve as unique fingerprints for signal source attribution.

The output space constitutes an open-set matching assignment where the number of antennas M and detected PCIs N may not be equal ($M \neq N$ generally), and the correspondence between visual devices and communication signals must be established without prior knowledge of the exact matching relationship. This open-world condition reflects real-world deployment scenarios.

The key challenges in this formulation include:

1. **Modality Gap**: The significant distributional differences between visual features and signal features create alignment difficulties.
2. **Data Scarcity**: Limited annotated multi-modal pairs for antenna-PCI correspondence, requiring data-efficient learning approaches.
3. **Open-World Complexity**: The variable number of antennas and signals per station, with potential missing detections or false positives in both modalities.
4. **Domain Specificity**: The absence of similar tasks in existing literature means pretrained models lack relevant inductive biases for this communication network application.

This task formulation distinguishes itself from conventional multi-modal learning problems by addressing the unique constraints of communication infrastructure, where visual and signal modalities must be correlated under practical deployment constraints to solve a concrete industrial problem.

3.2 Multi-modal Data Acquisition

As illustrated in Figure 1, our multi-modal dataset is constructed from three complementary sources, each providing a unique perspective on the antenna deployment and its radio characteristics.

Visual Data. High-resolution RGB image sequences of communication towers are captured by a drone performing a controlled orbit around each site. This procedure yields approximately 30 images per station, comprehensively documenting pole-mounted and rooftop antennas against diverse backgrounds. From these images, we extract individual antenna instances and estimate their key geometric features—azimuth (θ), length (L), width (W), height (H), and tilt (α)—using 3D reconstruction techniques (e.g., Structure-from-Motion). The visual modality is therefore represented as $\mathcal{V} = \{v_1, v_2, \dots, v_M\}$, where v_i is the feature vector encapsulating the i -th antenna’s appearance and geometry.

Signal Data. Concurrently, Physical Cell Identity (PCI) signal data is collected by performing radio frequency scans

on predefined 4G and 5G network frequencies. This dataset provides a set $\mathcal{S} = \{s_1, s_2, \dots, s_N\}$, where each signal s_j is characterized by its geographic coordinates (latitude ϕ_j , longitude λ_j) and signal intensity metrics, such as Reference Signal Received Power (RSRP).

Ground Truth Association. The core challenge of cross-modal matching requires a precise, verified link between visual antennas and their emitted signals. The ground truth affiliation for antenna v_i is established by associating its unique visual identifier (ID) with a corresponding PCI-level signal s_j , using standardized network reference data. This yields a set of verified matching pairs $\mathcal{P} = \{(v_a, s_b) \mid \text{antenna } v_a \text{ is affiliated with signal } s_b\}$, which serves as the supervision for our learning task.

3.3 Token Entropy Regularizer

A fundamental challenge in training multi-modal networks lies in aligning heterogeneous feature distributions. We hypothesize that dynamically measuring and regularizing the information encoding density of learned token representations can facilitate this alignment. To this end, we propose the Token Entropy Regularization (TER) module, a sparsity-inducing mechanism that encourages the model to form compact, high-fidelity representations by penalizing tokens with high entropy, those that are uniformly distributed and thus less informative.

Enhanced Token Entropy (ETE): Given the feature representation $\mathbf{F}_m \in \mathbb{R}^{T \times D}$ generated by the modality encoder E_m , where T denotes the number of tokens and D the feature dimension, we compute a probability distribution over the feature channels for each token. Specifically, for the t -th token $\mathbf{f}_{m,t} \in \mathbb{R}^D$, we apply the SoftMax function along the channel dimension to obtain a discrete probability distribution:

$$\mathbf{p}_{m,t} = \text{SoftMax}(\mathbf{f}_{m,t}) = \left[\frac{\exp(f_{m,t,i})}{\sum_{j=1}^D \exp(f_{m,t,j})} \right]_{i=1}^D \quad (1)$$

The token entropy $H_{m,t} \equiv H(\mathbf{f}_{m,t})$ is then calculated as the Shannon entropy of this distribution, yielding a scalar measure of the token’s feature complexity:

$$H_{m,t} = - \sum_{i=1}^D p_{m,t,i} \cdot \log(p_{m,t,i}) \quad (2)$$

A high entropy value indicates a token whose activations are evenly spread across feature channels, suggesting a less discriminative or “noisy” representation. Conversely, a low entropy value indicates a “sparse” token with activations concentrated on a few channels, typically associated with more specific, informative features.

To inject this self-awareness into the learning process, the scalar entropy $H_{m,t}$ is processed by a lightweight projection head (e.g., a linear layer followed by LayerNorm) and added back to the original token feature via a gated residual connection:

$$\tilde{\mathbf{f}}_{m,t} = \mathbf{f}_{m,t} + \gamma \cdot \text{LayerNorm}(\mathbf{W}H_{m,t} + \mathbf{b}), \quad (3)$$

where $\mathbf{W} \in \mathbb{R}^{D \times 1}$ and $\mathbf{b} \in \mathbb{R}^D$ are learnable parameters, and γ is a learnable scalar gate. The output of the ETE layer is the entropy-augmented feature matrix $\tilde{\mathbf{F}}_m = [\tilde{\mathbf{f}}_{m,1}, \tilde{\mathbf{f}}_{m,2}, \dots, \tilde{\mathbf{f}}_{m,T}]^\top$.

Token Entropy Loss (TEL). Beyond the architectural modification, we explicitly regularize token sparsity via an auxiliary loss. The TEL encourages the model to produce low-entropy, high-confidence tokens by minimizing the mean token entropy across the batch and modalities:

$$\mathcal{L}_{TEL} = \frac{1}{|\mathcal{B}|} \frac{1}{T} \sum_{m \in \{\mathcal{V}, \mathcal{S}, \mathcal{G}\}} \sum_{t=1}^T H_{m,t}, \quad (4)$$

where \mathcal{B} denotes the current training batch and $|\mathcal{B}|$ is its size. The total training objective becomes a weighted sum of the primary task loss (e.g., contrastive or matching loss) and the regularization term:

$$\mathcal{L}_{\text{total}} = \mathcal{L}_{\text{task}} + \lambda \mathcal{L}_{TEL}, \quad (5)$$

where λ is a hyperparameter controlling the strength of the entropy regularization. This formulation enables a principled trade-off between task performance and the compactness of the learned multi-modal representations.

4 Experiments

4.1 Implementation Details

Hyperparameter: All experiments were conducted on a single NVIDIA A800 GPU. We used the Adam optimizer for pretraining and AdamW for fine-tuning. The learning rate followed a cosine decay schedule, preceded by a linear warm-up phase spanning 10 epochs. Each training task ran for 200 epochs.

Fixed Encoders: The encoders for antenna geometric features and PCI signals are based on a modified Transformer architecture, with 4 layers, 8 attention heads, and a feature dimension of 1024.

4.2 Antenna Type Classification

Vision feature extraction: We evaluated multiple components of our multi-modal framework for antenna type classifications. For visual feature extraction, we compared DINOv3 (ViT-L/16 and ViT-H+/16 variants) with PVTv2, testing three token generation strategies: [CLS] token, top layer features (TLF) with global average pooling, and their fusion. Geometric features were encoded using relative position encoding and normalized, comparing 3D point clouds against abstract semantic representations. For multi-modal fusion, we evaluated cross-attention, self-attention, and MLP-based approaches.

As shown in Table 1, DINOv3 significantly outperforms PVTv2, with ViT-L/16 achieving the best results (86.4% accuracy using TLF). Semantic geometric features (86.4%)

Vision Encoder	Variant	Acc. (%)
PVTv2-b3	LAYER-3	67.5
PVTv2-b3	LAYER-ALL	68.8
ViT-H+/16	[CLS]	75.5
ViT-H+/16	[CLS]+TLF	74.9
ViT-H+/16	TLF	76.6
ViT-L/16	[CLS]	85.9
ViT-L/16	[CLS]+TLF	85.5
ViT-L/16	TLF	86.4
Geometric Features		
3D Points	-	84.6
Semantic Geometric	-	86.4
Fusion Method		
Cross-Attention	-	85.9
MLP	-	86.1
Self-Attention	-	86.4

Table 1: Comprehensive evaluation of vision encoders, geometric features, and fusion methods for antenna type classification. Best: DINOv3 (ViT-L/16) with TLF, semantic geometric encoding, and self-attention fusion.

proved more effective than raw 3D points (84.6%). Among fusion methods, self-attention achieved the highest accuracy (86.4%), though differences between fusion strategies were minimal. These results demonstrate that DINOv3 with semantic geometric features and self-attention fusion provides the optimal configuration for our task.

4.3 Antenna Affiliation Pretraining

We evaluate the contribution of the proposed Token Entropy Regularization (TER) module by conducting comparative experiments with three modified visual encoders: TimeSformer, Video Swin Transformer, and ViViT. As shown in Table 2, the TER module consistently improved the accuracy of all three architectures, demonstrating that its mechanism for explicitly modeling token complexity effectively enhances feature representations. The Video Swin Transformer achieved the highest performance, with a top-1 accuracy of 65.12% when full TER regularization was applied.

Vision Encoder	Config	Acc@1	Acc@3
TimeSformer	Baseline	53.49	88.37
	+ TER	62.79	95.35
ViViT	Baseline	51.16	88.37
	+ TER	53.49	90.70
Video Swin	Baseline	55.81	86.05
	+ TER	65.12	86.05

Table 2: Comprehensive evaluation of token entropy regularizer module across different visual encoders in pretraining.

4.4 Integrated Antenna Affiliation Evaluation

We evaluated the practical efficacy of our method by comparing two training paradigms: End-to-End (End2End) learning and supervised fine-tuning on the pretrained model (Pretrain

+ SFT). Results on real-world 4G/5G antenna-PCI matching data (Table 3) show that the Pretrain + SFT paradigm substantially and consistently outperforms the End2End approach across all three video encoder architectures. This universal improvement, with top-1 accuracy gains ranging from approximately +26% (Video Swin) to +38% (TimeSformer), validates the critical advantage of the proposed pretraining stage. Under this superior paradigm, the Video Swin encoder achieves the best performance, with an overall top-1 accuracy of 87.91% and a top-3 accuracy of 91.94%.

4.5 Visualization

The following visualizations provide qualitative insights into model performance for the antenna type classification and matching tasks.

Figure 3 compares the antenna type classification results of three different models against ground truth annotations. The visualization uses a consistent encoding scheme: solid and dashed lines represent antennas from Company A and Company B, respectively, while blue and red colors denote low-frequency and high-frequency variants. This structured comparison reveals systematic differences in classification accuracy across models.

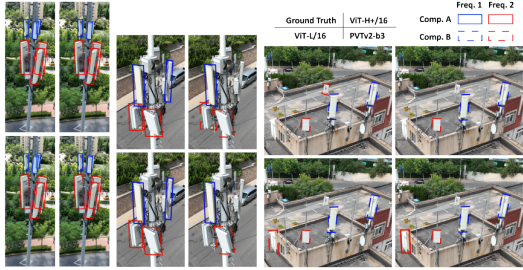


Figure 3: Visual comparison of antenna type classification. Rows show different antenna instances; columns compare ground truth (left) with predictions from three distinct models. Line style indicates manufacturer (solid: Company A, dashed: Company B); color indicates frequency band (blue: low, red: high).

Figure 4 visualizes antenna affiliation matching performance in complex urban environments. Detected PCI signals (yellow points) are overlaid on scenario backgrounds, with solid circles representing correctly matched signals and dashed circles indicating unclassified or ambiguous detections. Circle colors correspond to specific signal classes. The visualization demonstrates the model’s capability to maintain accurate signal-source associations across challenging real-world conditions.

4.6 Ablation Study

Pretraining stage: As shown in Figure 5, the ETE module (red) accelerates convergence and achieves higher final accuracy compared to the baseline (blue). The complete TER method, which incorporates the TEL constraint (green), delivers the best performance. This indicates that token-level complexity perception enables the model to learn more effective and adaptive feature representations.

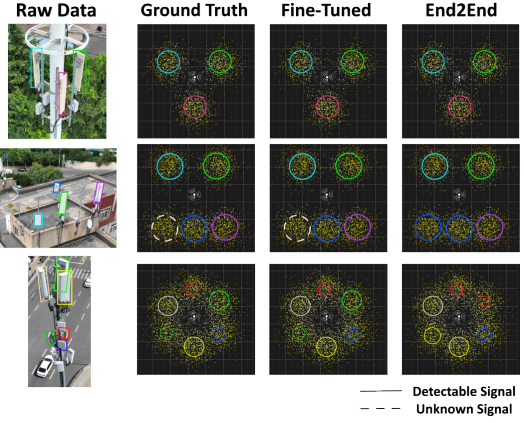


Figure 4: Antenna affiliation matching results. Each row presents a distinct urban scenario with communication infrastructure. Yellow points mark detected PCI signals, with solid circles indicating verified matches and dashed circles indicating unclassified signals. Colors represent different signal classes.

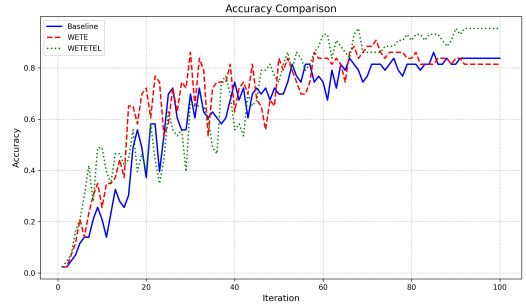


Figure 5: Accuracy during pretraining. Our proposed ETE module converges faster and to a higher accuracy than the baseline. Performance is further improved by the full TER method (ETE + TEL).

Analysis of First Token Entropy in Pretraining: To investigate how the proposed TER module contributes to the adaptive sparse rate encoding, we analyzed the evolution of first token entropy for each modality during pretraining. The first token is selected due to the attention sink property of current attention mechanisms, as shown in Figure 6 (D), making it particularly informative for measuring representation complexity [Xiao *et al.*, 2023]. As shown in Figure 6 (A-C), we tracked first token entropy for each modality (PCI signal, image, geometric vector) over 100 epochs under different regularization conditions.

The analysis yields two principal findings that align with the goal of learning sparse, informative representations. First, the significant disparity in baseline entropy across modalities underscores their inherent differences in representation complexity, highlighting the need for an adaptive sparsification strategy. Second, the figure demonstrates a clear, modality-dependent effect on entropy modulation, effectively achieving the “adaptive” sparsity desired by compressing complex representations while preserving essential information.

Video Encoder	Training Paradigm	4G Accuracy (%)		5G Accuracy (%)		Overall	
		@1	@3	@1	@3	@1	@3
TimeSformer	End2End	30.43	65.22	30.30	63.64	30.36	64.29
ViViT	End2End	52.17	86.96	60.61	84.85	56.39	85.91
Video Swin	End2End	51.52	86.96	72.73	90.91	62.12	89.93
TimeSformer	Pretrain + SFT	69.56	86.95	66.66	74.07	68.11	80.51
ViViT	Pretrain + SFT	78.26	91.30	81.48	85.18	79.87	88.24
Video Swin	Pretrain + SFT	86.95	91.30	88.88	92.59	87.91	91.94

Table 3: Comprehensive evaluation of antenna-PCI matching performance across video encoders and training paradigms, showing both @1 and @3 accuracy metrics. TER framework consistently improves performance across all metrics, with ViViT achieving optimal results.

Method	i2t.R@1	i2t.R@5	i2t.R@10	t2i.R@1	t2i.R@5	t2i.R@10
CLS Setting						
Baseline	0.5040	0.7986	0.8705	0.4797	0.7991	0.8700
+ TER	0.5027 (-0.25%)	0.8023 (+0.46%)	0.8737 (+0.37%)	0.4790 (-0.15%)	0.7958 (-0.40%)	0.8697 (-0.03%)
Non-CLS Setting						
Baseline	0.5077	0.7949	0.8737	0.4869	0.8013	0.8730
+ TER	0.5121 (+0.88%)	0.8114 (+2.08%)	0.8791 (+0.62%)	0.4998 (+2.64%)	0.8080 (+0.83%)	0.8772 (+0.48%)

Table 4: Performance comparison on Flickr8K dataset with and without TER regularization. Values represent recall metrics with improvement percentages shown in parentheses.

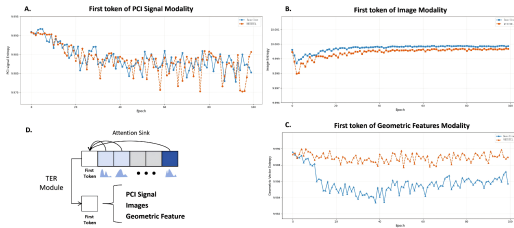


Figure 6: Dynamics of first-token entropy under regularization settings. (A-C) Entropy trajectories for the PCI signal, image, and geometric feature modalities, illustrating the adaptive sparsification effect of the TER module during pretraining. (D) Schematic representation of the first token in the token entropy regularization framework.

4.7 Token Entropy Regularizer Generalization

To evaluate the generalization capability of the proposed TER method, we conducted 100-epoch training experiments on the Flickr8K dataset under two distinct settings: CLS token-based representation and non-CLS token representation. The results demonstrate the adaptive sparsification effect of our approach across different architectural configurations. Quantitative results are summarized in Table 4.

CLS Token Usage: Under the CLS token setting, the TER-regularized model exhibits mixed performance compared to the baseline. While image-to-text recall at 5 (i2t.R@5) improves by +0.46% and i2t.R@10 increases by +0.37%, other metrics show minor declines, with the largest drop observed in t2i.R@5(-0.40%). This indicates that CLS-based representations, which aggregate global information into a single token, may not fully leverage the token-wise sparsification induced by TER.

Non-CLS Token Usage: In contrast, the non-CLS set-

ting demonstrates consistent improvements across all evaluation metrics. The TER-regularized model achieves significant gains in text-to-image recall at 1 (t2i.R@1) with an improvement of +2.64% and image-to-text recall at 5 (i2t.R@5) with +2.08% improvement. This performance enhancement aligns with the core principle of our TER approach, which promotes sparse, informative representations at the token level rather than relying on aggregated CLS embeddings. The results indicate that by preserving fine-grained token-level information while applying entropy constraints, the model learns more discriminative representations for cross-modal retrieval tasks.

5 Conclusion

This paper introduced a novel multimodal framework for automated antenna affiliation identification, enhanced by a token-level regularizer. By synergistically fusing visual data from drone-captured imagery with 4G/5G network signals, the proposed system overcomes critical limitations of conventional manual methods. Experimental results validate the framework's efficacy, demonstrating substantial improvements from the proposed Token Entropy Regularization. These advancements provide significant practical benefits for telecommunication infrastructure management, enabling more efficient network planning, operational optimization, and asset management while mitigating the safety risks inherent in manual field verification.

References

[Abozariba *et al.*, 2025] R. Abozariba, M. S. Islam, J. Hayes, A. A. Bipon, A. Aneiba, B. B. Cebecioglu, A. T. Asyhari, D. Mi, P. Xiao, and C. L. Wang. Street-level cellular networks monitoring in the 5G era. In *2025 IEEE 22nd Consumer Communications & Networking Conference (CCNC)*, pages 1–7. IEEE, January 2025.

[Aliu *et al.*, 2012] Osianoh G. Aliu, Ali Imran, Muhammad A. Imran, and Barry Evans. A survey of self organisation in future cellular networks. *IEEE Communications Surveys & Tutorials*, 15(1):336–361, 2012.

[Arnab *et al.*, 2021] Anurag Arnab, Mostafa Dehghani, Georg Heigold, Chen Sun, Mario Lučić, and Cordelia Schmid. Vivit: A video vision transformer. *arXiv preprint arXiv:2103.15691*, 2021.

[Bertasius *et al.*, 2021] Gedas Bertasius, Heng Wang, and Lorenzo Torresani. Is space-time attention all you need for video understanding? *arXiv preprint arXiv:2102.05095*, 2021.

[Bolya and Hoffman, 2023] Daniel Bolya and Judy Hoffman. Token merging for fast stable diffusion. In *Proceedings of the IEEE/CVF Conference on Computer Vision and Pattern Recognition*, pages 4599–4603, 2023.

[Chen *et al.*, 2024] Hongyu Chen, Zhen Lai, Hongyi Zhang, Xin Wang, Marc Eichner, Kaizhao You, Meng Cao, Bowen Zhang, Yifei Yang, and Zhe Gan. Contrastive localized language-image pre-training. *arXiv preprint arXiv:2410.02746*, October 2024.

[Cheng *et al.*, 2024] Daixuan Cheng, Yuxian Gu, Shaohan Huang, Jing Bi, Minlie Huang, and Furu Wei. Instruction pre-training: Language models are supervised multitask learners. *arXiv preprint arXiv:2406.14491*, June 2024.

[Correia *et al.*, 2019] Gonçalo M. Correia, Vlad Niculae, and André F. T. Martins. Adaptively sparse transformers. *arXiv preprint arXiv:1909.00015*, September 2019.

[Dosovitskiy *et al.*, 2020] Alexey Dosovitskiy, Lucas Beyer, Alexander Kolesnikov, Dirk Weissenborn, Xiaohua Zhai, Thomas Unterthiner, Mostafa Dehghani, Matthias Minderer, Georg Heigold, Sylvain Gelly, Jakob Uszkoreit, and Neil Houlsby. An image is worth 16x16 words: Transformers for image recognition at scale. *arXiv preprint arXiv:2010.11929*, 2020.

[Fan *et al.*, 2021] Haoqi Fan, Bo Xiong, Karttikeya Mangalam, Yanghao Li, Zhicheng Yan, Jitendra Malik, and Christoph Feichtenhofer. Multiscale vision transformers. In *Proceedings of the IEEE/CVF International Conference on Computer Vision*, pages 6824–6835, 2021.

[Gao *et al.*, 2025] Leo Gao, Ananth Rajaram, James Coxon, Shreeya V. Govande, Bowen Baker, and Daniel Mossing. Weight-sparse transformers have interpretable circuits. *arXiv preprint arXiv:2511.13653*, November 2025.

[Girdhar *et al.*, 2023] Rohit Girdhar, Alaaeldin El-Nouby, Zhuang Liu, Mannat Singh, Kalyan Vasudev Alwala, Armand Joulin, and Ishan Misra. Imagebind: One embedding space to bind them all. In *Proceedings of the IEEE/CVF Conference on Computer Vision and Pattern Recognition*, pages 15180–15190, 2023.

[He *et al.*, 2022] Kaiming He, Xinlei Chen, Saining Xie, Yanghao Li, Piotr Dollár, and Ross Girshick. Masked autoencoders are scalable vision learners. In *Proceedings of the IEEE/CVF Conference on Computer Vision and Pattern Recognition*, pages 16000–16009, 2022.

[Hu *et al.*, 2024] Y. Hu, D. Zou, and D. Xu. An in-depth investigation of sparse rate reduction in transformer-like models. *Advances in Neural Information Processing Systems*, 37:116815–116837, 2024.

[Huang *et al.*, 2024] Zhicheng Huang, Qihang Ye, Bingyi Kang, Jiashi Feng, and Heng Fan. Classification done right for vision-language pre-training. *Advances in Neural Information Processing Systems*, 37:96483–96504, 2024.

[Liu *et al.*, 2021] Ze Liu, Yutong Lin, Yue Cao, Han Hu, Yixuan Wei, Zheng Zhang, Stephen Lin, and Baining Guo. Swin transformer: Hierarchical vision transformer using shifted windows. In *Proceedings of the IEEE/CVF International Conference on Computer Vision (ICCV)*, pages 10012–10022, 2021.

[Liu *et al.*, 2022a] Ze Liu, Jia Ning, Yue Cao, Yixuan Wei, Zheng Zhang, Stephen Lin, and Han Hu. Video swin transformer. *arXiv preprint arXiv:2106.13230*, 2022.

[Liu *et al.*, 2022b] Zhuang Liu, Hanzi Mao, Chao-Yuan Wu, Christoph Feichtenhofer, Trevor Darrell, and Saining Xie. A convnet for the 2020s. In *Proceedings of the IEEE/CVF Conference on Computer Vision and Pattern Recognition*, pages 11976–11986, 2022.

[Liu *et al.*, 2025] Zhenyu Liu, Dong Yang, Minghui Zhang, Haoran Sun, Haonan Wu, Hao Wang, Weiming Shen, Chengliang Chai, and Shuo Xia. SeLIP: Similarity enhanced contrastive language image pretraining for multimodal head MRI. *arXiv preprint arXiv:2503.19801*, March 2025.

[Marin *et al.*, 2021] D. Marin, J.H.R. Chang, A. Ranjan, A. Prabhu, M. Rastegari, and O. Tuzel. Token pooling in vision transformers. *arXiv preprint arXiv:2110.03860*, 2021.

[Narmanlioglu and Zeydan, 2018] Omer Narmanlioglu and Engin Zeydan. Mobility-aware cell clustering mechanism for self-organizing networks. *IEEE Access*, 6:65405–65417, 2018.

[Omri *et al.*, 2025] Yasmine Omri, others, and Stanford. Token sequence compression for efficient multimodal computing. *arXiv preprint*, 2025.

[Oquab *et al.*, 2023] Maxime Oquab, Timothée Darcet, Theo Moutakanni, Huy Vo, Marc Szafraniec, Vasil Khalidov, Pierre Fernandez, Daniel Haziza, Francisco Massa, Alaaeldin El-Nouby, et al. Dinov3: Learning robust visual features without supervision. *arXiv preprint arXiv:2304.07193*, 2023.

[Plested and Gedeon, 2022] James Plested and Tom Gedeon. Deep transfer learning for image classification: A survey. *arXiv preprint arXiv:2205.09904*, May 2022.

[Qi *et al.*, 2017] Yihong Qi, Guangliang Yang, Liang Liu, Jun Fan, Antonio Orlandi, He Kong, Wenxian Yu, and Zhihang Yang. 5G over-the-air measurement challenges: Overview. *IEEE Trans. Electromagn. Compat.*, 59(6):1661–1670, 2017.

[Radford *et al.*, 2021] Alec Radford, Jong Wook Kim, Chris Hallacy, Aditya Ramesh, Gabriel Goh, Sandhini Agarwal, Girish Sastry, Amanda Askell, Pamela Mishkin, Jack Clark, et al. Learning transferable visual models from natural language supervision. *arXiv preprint arXiv:2103.00020*, 2021.

[Shoaib *et al.*, 2024] Muhammad Shoaib, Ghazanfar Husnain, Nadeem Sayed, and Sungmook Lim. Unveiling the 5G frontier: Navigating challenges, applications, and measurements in channel models and implementations. *IEEE Access*, 12:59533–59560, 2024.

[Singh *et al.*, 2022] Mannat Singh, Laura Gustafson, Aaron Adcock, Vinicius de Freitas Reis, Bugra Gedik, R. Pranav Kosaraju, Dhruv Mahajan, Ross Girshick, Piotr Dollár, and Laurens Van Der Maaten. Revisiting weakly supervised pre-training of visual perception models. In *Proceedings of the IEEE/CVF Conference on Computer Vision and Pattern Recognition (CVPR)*, pages 804–814, 2022.

[Song and others, 2024] Dingjie Song et al. Less is more: A simple yet effective token reduction method for efficient multi-modal llms. In *Proceedings of the 29th International Conference on Computational Linguistics*, pages –, 2024. The Chinese University of Hong Kong, Shenzhen.

[Tolstikhin *et al.*, 2021] Ilya O Tolstikhin, Neil Houlsby, Alexander Kolesnikov, Lucas Beyer, Xiaohua Zhai, Thomas Unterthiner, Jessica Yung, Andreas Steiner, Daniel Keysers, Jakob Uszkoreit, and Mario Lucic. Mlp-mixer: An all-mlp architecture for vision. *Advances in neural information processing systems*, 34:24261–24272, 2021.

[Touvron *et al.*, 2021] Hugo Touvron, Matthieu Cord, Matías Douze, Francisco Massa, Alexandre Sablayrolles, and Hervé Jégou. Training data-efficient image transformers and distillation through attention. In *International conference on machine learning*, pages 10347–10357. PMLR, 2021.

[Vaswani *et al.*, 2017] Ashish Vaswani, Noam Shazeer, Niki Parmar, Jakob Uszkoreit, Llion Jones, Aidan N Gomez, Łukasz Kaiser, and Illia Polosukhin. Attention is all you need. *Advances in Neural Information Processing Systems*, 30:5998–6008, 2017.

[Wang and others, 2025] S. Wang et al. Beyond the 80/20 rule: High-entropy minority tokens drive effective reinforcement learning for LLM reasoning. *arXiv preprint arXiv:2506.01939*, 2025.

[Wang *et al.*, 2015] Xianbin Wang, Xi Li, and Victor C. Leung. Artificial intelligence-based techniques for emerging heterogeneous network: State of the arts, opportunities, and challenges. *IEEE Access*, 3:1379–1391, 2015.

[Wang *et al.*, 2021] Wenhai Wang, Enze Xie, Xiang Li, Deng-Ping Fan, Kaitao Song, Ding Liang, Tong Lu, Ping Luo, and Ling Shao. Pyramid vision transformer: A versatile backbone for dense prediction without convolutions. *arXiv preprint arXiv:2102.12122*, 2021.

[Wang *et al.*, 2022] Wenhai Wang, Enze Xie, Xiang Li, Deng-Ping Fan, Kaitao Song, Ding Liang, Tong Lu, Ping Luo, and Ling Shao. Pvt v2: Improved baselines with pyramid vision transformer. *Computational Visual Media*, 8(3):1–10, 2022.

[Wang *et al.*, 2025] Hongjie Wang, Chen Ju, Weilin Lin, Siyu Xiao, Mingda Chen, Yu Huang, Chuanyi Liu, Ming Yao, Jiayi Lan, Yang Chen, and Qiang Liu. Advancing myopia to holism: Fully contrastive language-image pre-training. In *Proceedings of the IEEE/CVF Conference on Computer Vision and Pattern Recognition (CVPR)*, pages 29791–29802, 2025.

[Wu *et al.*, 2023] Yangjun Wu, Kebin Fang, Dongxiang Zhang, Han Wang, Hao Zhang, and Gang Chen. Tlm: Token-level masking for transformers. *arXiv preprint arXiv:2310.18738*, 2023.

[Xiao *et al.*, 2023] Guangxuan Xiao, Yuandong Tian, Beidi Chen, Song Han, and Mike Lewis. Efficient streaming language models with attention sinks. *arXiv preprint arXiv:2309.17453*, 2023.

[Yao *et al.*, 2024] Y. Yao, Z. Li, and H. Zhao. SIR-LLM: Streaming infinite retentive LLM. *arXiv preprint arXiv:2405.12528*, 2024.

[Yu *et al.*, 2017] Xin Yu, Tongliang Liu, Xinchao Wang, and Dacheng Tao. On compressing deep models by low rank and sparse decomposition. In *Proceedings of the IEEE Conference on Computer Vision and Pattern Recognition*, pages 7370–7379, 2017.

[Yu *et al.*, 2023] Y. Yu, S. Buchanan, D. Pai, T. Ryu, J. Wu, M. Monge, M. Li, B. Sun, Y. Sun, T. Sun, et al. White-box transformers via sparse rate reduction. *Advances in Neural Information Processing Systems*, 36:9422–9457, 2023.

[Zeng *et al.*, 2025] F. Zeng, D. Yu, Z. Kong, and H. Tang. Token transforming: A unified and training-free token compression framework for vision transformer acceleration. *arXiv preprint arXiv:2506.05709*, 2025.

[Zhai *et al.*, 2023] Xiaohua Zhai, Basil Mustafa, Alexander Kolesnikov, and Lucas Beyer. Sigmoid loss for language image pre-training. *arXiv preprint arXiv:2303.15343*, 2023.

[Zhao *et al.*, 2021] Hengshuang Zhao, Li Jiang, Jiaya Jia, Philip HS Torr, and Vladlen Koltun. Point transformer. In *Proceedings of the IEEE/CVF International Conference on Computer Vision*, pages 16259–16268, 2021.

[Zhu *et al.*, 2015] Shuyuan Zhu, Bing Zeng, and Moncef Gabbouj. Adaptive sampling for compressed sensing based image compression. *Journal of Visual Communication and Image Representation*, 30:94–105, 2015.